Nonlinear Stability and Saturation of Ballooning Modes in Tokamaks*

C. J. Ham,† S. C. Cowley,‡ and G. Brochard‡
CCFE, Culham Science Centre, Abingdon, Oxfordshire OX14 3DB, United Kingdom

H. R. Wilson
York Plasma Institute, Department of Physics, University of York, Heslington, York YO10 5DD, United Kingdom
(Received 15 December 2015; revised manuscript received 4 February 2016; published 9 June 2016)

The theory of tokamak stability to nonlinear "ballooning" displacements of elliptical magnetic flux tubes is presented. Above a critical pressure profile the energy stored in the plasma may be lowered by finite (but not infinitesimal) displacements of such tubes (metastability). Above a higher pressure profile, the linear stability boundary, such tubes are linearly and nonlinearly unstable. The predicted saturated flux tube displacement can be of the order of the pressure gradient scale length. Plasma transport from these displaced flux tubes may explain the rapid loss of confinement in some experiments.

DOI: 10.1103/PhysRevLett.116.235001

Fast magnetohydrodynamic (MHD) instabilities limit the pressure (beta) in magnetically confined fusion plasmas. The limit is observed to be one of two kinds, either a soft limit where the instability limits the pressure to a critical profile or a hard limit where the instability rapidly destroys confinement and releases enough stored energy to take the system well below the critical pressure profile. Sometimes the instability terminates the discharge entirely [1]. There are also two kinds of MHD instability: large scale kink instabilities and small scale, field aligned ballooning instabilities [2]. It is often supposed that ballooning instabilities provide a soft limit, especially near the plasma edge [3]. Some observations of the pressure profile evolution in the pedestal, a steep pressure gradient region at the edge of some tokamak discharges, are consistent with a soft ballooning limit [4,5]. However, *edge-localized modes* (ELMs), instabilities of the pedestal, cause an explosive eruption of multiple fine scale flux tubes and a rapid loss of edge confinement [6]. This suggests that ballooning instabilities can sometimes provide a hard limit to edge confinement. When then is the ballooning beta limit hard and when is it soft?

In this Letter we provide a general theory of the nonlinear stability of ballooning modes. We argue that without dissipation the nonlinear consequence of ballooning modes is the eruption of isolated elliptical magnetic flux tubes. Certainly such elliptical erupting tubes are the long time limit of the weakly nonlinear theory developed in [7,8]. The explosive dynamics and metastability of such tubes in one-dimensional line tied gravitational equilibria were studied in [9]. Here, we calculate the dynamics and final saturated states of erupting flux tubes, first in general [Eqs. (2) and (3)] and then (as an example) in a simple large aspect ratio tokamak with nearly circular flux surfaces. The equilibrium contains a region of steep pressure gradient, a transport barrier, where the pressure gradient is of the order of the critical gradient for linear stability. We adopt this equilibrium since it yields a simple nonlinear generalization of the s-α linear ballooning model of [10] and so illustrates the nonlinear dynamics. Specifically, it illustrates the metastability of some linearly stable equilibria. Metastability is a phenomenon encountered in many physical systems and indeed it is clear from this Letter and from Ref. [9] that many confined plasmas are also metastable. However, despite its importance, metastability in confined plasmas is largely unexplored.

Equilibrium and equations.—We represent the tokamak equilibrium in flux coordinates: ϕ is the toroidal angle, r is a radiuslike variable that is constant on a magnetic surface, and θ is a poloidal angle chosen to make the field lines "straight"—see [11,12]. Thus, we choose $r(\nabla r \times \nabla\theta) = R_0\nabla\phi$, where R_0 is the cylindrical radius of the magnetic axis. Then

$$\mathbf{B}_0 = -\bar{B}_0 R_0\{f(r)\nabla r \times \nabla\mathcal{S}\}, \tag{1}$$

where $\bar{B}_0$ is a constant, $\mathcal{S} = \phi - q(r)[\theta - \theta_0(r)]$, $q(r)$ is the safety factor, and $\theta_0(r)$ is an arbitrary function of r. We assume the tokamak has a large aspect ratio (i.e., $r/R_0 = \epsilon \ll 1$) and low beta $p_0(r) \sim O(\epsilon^2\bar{B}_0^2)$. The

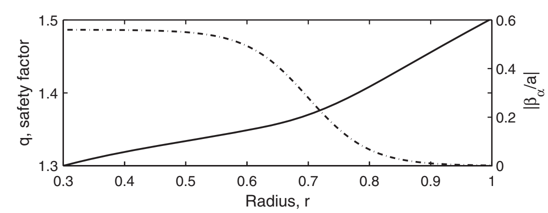

FIG. 1. Profile of safety factor q (solid line, left-hand axis) and normalized pressure $\beta_\alpha/a = 2\mu_0 R_0 q^2 p_0(r)/B_0^2 a$ (dashed line, right-hand axis) for the internal transport barrier (where a is the plasma minor radius).

*For further information on this paper contact PublicationsManager@ccfe.ac.uk.

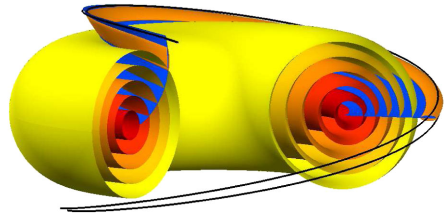

FIG. 2. Elliptical (orange) flux tube with $\Delta r \sim \delta_2 \gg \Delta \mathcal{S} \sim \delta_1$ sliding along (blue) surface $\mathcal{S} = 0$ parting surrounding (black) field lines. Note that the tube's displacement, $\xi = r - r_0$, is larger on the large R part of the flux surfaces—the tube balloons. The magnetic shear ($s = rq'/q$) causes the twist and narrowing of the tube on the inside.

transport barrier is a narrow region of steep pressure gradient $[rp_0' \sim O(p_0/\epsilon)]$ of width $\sim\epsilon r$ centered around a surface $r = r_p$; see Fig. 1. The equilibrium is obtained from an expansion in ϵ (as in [12]).

We consider a highly elliptical flux tube of widths Δr and $\Delta\mathcal{S}$ with $r \gg \Delta r \sim \delta_2 \gg \Delta\mathcal{S} \sim \delta_1$ whose center originates in the field line on the flux surface labeled by r_0 and $\mathcal{S} = 0$. The field lines in the tube are displaced along the surface $\mathcal{S} = 0$ with shape given by $r = r(\theta, r_0, t) = \xi + r_0$, where $r(t=0) = r_0$; see Fig. 2.

In principle, we could consider motion along any $\mathcal{S}$ surface defined by any function $\theta_0(r)$; we restrict ourselves to the choice $\theta_0(r) = 0$. This is the choice for the most linearly unstable motions. The tube wraps around the torus many times and we consider $r(\theta, r_0, t)$ on the domain $-\infty < \theta < \infty$. We ignore the fact that the $\mathcal{S} = 0$ surface intersects itself as θ increases since we assume that the perturbations are sufficiently localized in θ to avoid self intersection of the flux tube. The plasma is taken to be perfectly conducting—i.e., the plasma is frozen to the field. Thus, the field lines must remain attached to their original surfaces and therefore $r = r(\theta, r_0, t) \to r_0$ as $|\theta| \to \infty$. The derivation of the equation of motion here follows the treatment for a general equilibrium of a magnetically confined plasma in Appendix B of [13]. The exact shape of the tube is not needed but we do assume that δ_1 is sufficiently small that we can treat the field and pressure outside the tube as unperturbed.

We denote the field inside the tube to be $\mathbf{B}_{\rm in} = \mathbf{B}_{\rm in}(\theta, r_0, t)$. The motion of the tube is assumed to be slow compared to the (sound) time to equalize pressure along the tube and thus the pressure in the tube is $p_{\rm in}(\theta, r_0, t) = p_0(r_0)$. The pressure forces across the tube in the direction of $\nabla\mathcal{S}$ are formally large ($\sim p_0/\delta_1$) and therefore the total pressure inside the tube must equal the total pressure just outside the tube. Thus,

$$B_{\rm in}^2(\theta, r_0, t) = B_0^2(\theta, r) + 2\mu_0[p_0(r) - p_0(r_0)], \quad (2)$$

where the small perturbations of the field and pressure outside the tube are neglected [this requires $1 \gg (\xi^2/R_0^2)(\delta_1^2/\delta_2^2)$]. The ideal MHD force $F_\perp$ pushing the field line along $\mathcal{S}$ in the direction $\mathbf{e}_\perp = (\nabla\mathcal{S} \times \mathbf{B}_0)/B_0$ is

$$F_\perp = \frac{1}{\mu_0}\left[\mathbf{B}_{\rm in}\cdot\nabla\mathbf{B}_{\rm in} - \nabla\left(\frac{B_{\rm in}^2}{2} + \mu_0 p_{\rm in}\right)\right]\cdot\mathbf{e}_\perp$$
$$= \frac{1}{\mu_0}[\mathbf{B}_{\rm in}\cdot\nabla\mathbf{B}_{\rm in} - \mathbf{B}_0\cdot\nabla\mathbf{B}_0]\cdot\mathbf{e}_\perp. \quad (3)$$

The second expression follows from Eq. (2) and the unperturbed equilibrium relation $\nabla(B_0^2/2 + \mu_0 p_0) = \mathbf{B}_0\cdot\nabla\mathbf{B}_0$. Equation (3) is valid when the tube is sufficiently elliptical so that $\delta_1^2 \ll \delta_2^3/\xi$. The expression in Eq. (3) is a generalized form of Archimedes' principle where the net force is the curvature force of the tube minus the curvature force of the tube it has displaced. Equations (2) and (3) express the physics determining nonlinear ballooning—the rest of the theory is geometry. By requiring that $\mathbf{B}_{\rm in}$ lie on $\mathcal{S}$, $F_\perp$ can in general be expressed in terms of $r(\theta, r_0, t)$ and its first and second derivatives with respect to θ at constant r_0; see Appendix B of [13]. When $r - r_0 = \xi$ is infinitesimal $F_\perp$ reduces to the familiar linear ballooning operator of [2]—see [13]. Note that the nonlinear force on each field line is determined independently. The equilibrium states of the field line satisfy $F_\perp(r(\theta, r_0, t)) = 0$. We model the dynamics of the tube by a simple drag evolution with $\mathbf{v} = v\mathbf{e}_\perp$, $F_\perp = \nu\mathbf{v}\cdot\mathbf{e}_\perp$, and $v = -R_0 f(\partial r/\partial t)$. The actual dynamics of the tube are clearly more complicated but the equilibrium states must, of course, satisfy $F_\perp(r(\theta, r_0, t)) = 0$. After some algebra we obtain from Eq. (3) the evolution equation for each field line $[r(\theta, r_0, t)]$ in our simple large aspect ratio model,

$$\nu'\left(\frac{\partial r}{\partial t}\right)[1 + (\alpha\sin\theta - s\theta)^2] = F_\perp'(r(\theta, r_0, t))$$
$$= (\beta_\alpha(r_0) - \beta_\alpha(r))[\cos\theta + \sin\theta(s\theta - \alpha\sin\theta)]$$
$$+ \left(\frac{\partial}{\partial\theta}\right)_{r_0}\left([1 + (\alpha\sin\theta - s\theta)^2]\left(\frac{\partial r}{\partial\theta}\right)_{r_0}\right)$$
$$-\frac{1}{2}\left(\frac{\partial r}{\partial\theta}\right)_{r_0}^2\left(\frac{\partial}{\partial r}\right)_\theta(\alpha\sin\theta - s\theta)^2, \quad (4)$$

where $\nu' = \nu\mu_0(q^2R_0^2/B_0^2)$, $F_\perp' = F_\perp\mu_0(qR_0^2 r/B_0^2)$, $s = rq'(r)/q(r)$, $\beta_\alpha(r) = 2\mu_0 R_0 q^2 p_0(r)/\bar{B}_0^2$, and $\alpha(r) = -d\beta_\alpha(r)/dr$. Equation (4) is a nonlinear generalization of the s-α model of [10]. We define the energy functional, $\mathcal{E}(r, r_0) = \int_{-\infty}^{\infty}\mathbf{B}_{\rm in}\cdot d\mathbf{r}$, where the integral is taken along the perturbed field line [13]. Note that $\mathcal{E}(r, r_0)$ is formally infinite but we can make it finite by subtracting the unperturbed value $\Delta\mathcal{E}(r, r_0) = \mathcal{E}(r, r_0) - \mathcal{E}(r_0, r_0)$. Drag evolution takes the flux tube to minima of the energy $\Delta\mathcal{E}(r, r_0)$; see [13]. The equilibrium states are stationary points of the variation of $\Delta\mathcal{E}(r, r_0)$ with respect to $r(\theta, r_0, t)$ at fixed r_0 [13]. The relative energy for our model is

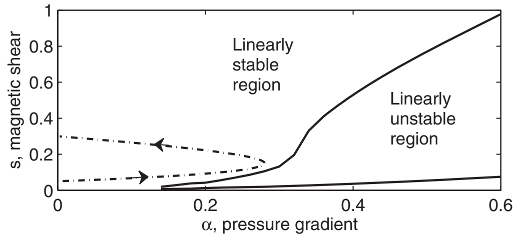

FIG. 3. *s*-*α* diagram showing the linear stability boundary [10]. The equilibrium here follows the trajectory of the dash-dotted line as r_0 is increased. The profile is linearly stable.

$$\Delta\mathcal{E}(r,r_0) = \int_{-\infty}^{\infty} d\theta\left[\frac{1}{2}\left(\frac{\partial r}{\partial\theta}\right)^2_{r_0}[1+(\alpha\sin\theta - s\theta)^2]\right] - \int_{-\infty}^{\infty} d\theta[\mathcal{A}(r,r_0)\cos\theta + \mathcal{B}(r,r_0)\theta\sin\theta - \mathcal{C}(r,r_0)\sin^2\theta], \quad (5)$$

where the integral is at fixed r_0 and the energy coefficients are $\mathcal{A}(r,r_0) = \int_{r_0}^{r}[\beta_\alpha(r') - \beta_\alpha(r_0)]dr'$, $\mathcal{B}(r,r_0) = \int_{r_0}^{r}[\beta_\alpha(r') - \beta_\alpha(r_0)]s(r')dr'$, and $\mathcal{C}(r,r_0) = \frac{1}{2}[\beta_\alpha(r) - \beta_\alpha(r_0)]^2$.

A linearly stable case.—We investigate a case where we choose profiles of $\alpha(r)$ and $s(r)$ that yield an internal transport barrier: $\alpha(r) = \alpha_0 \mathrm{sech}^2[(r - r_\alpha)/\epsilon_p]$ and $s(r) = (s_0 + s_1)/2 + [(s_1 - s_0)/2]\tanh[(r - r_s)/\epsilon_p]$. Linearizing Eq. (4) with $r = \xi(\theta, r_0, t) + r_0$ with $\xi\alpha', \xi s' \ll 1$ we obtain growing eigenmodes if the local values of $\alpha(r_0)$ and $s(r_0)$ lie in the unstable region of the *s*-*α* diagram [10]—see Fig. 3.

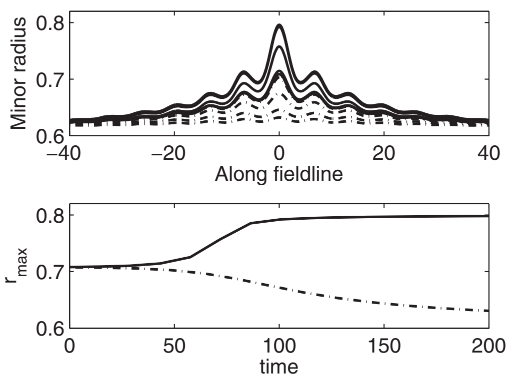

FIG. 4. The upper plot shows the shape of the field line at different times, $r = r(\theta, r_0, t)$ for $r_0 = 0.61$. The solid lines start with the initial condition just greater than the unstable equilibrium state r_{crit} and evolve upwards. The dash-dotted lines start with the initial condition just less than the unstable equilibrium state r_{crit} and evolve downwards. The final state of this evolution is the unperturbed field line. The lower plot shows the time evolution of the maximum value along the field line $r_{\max}(t) = r(0, r_0, t)$. Again, the solid (dash-dotted) line starts with the initial condition just greater (just less) than the unstable equilibrium state r_{crit}.

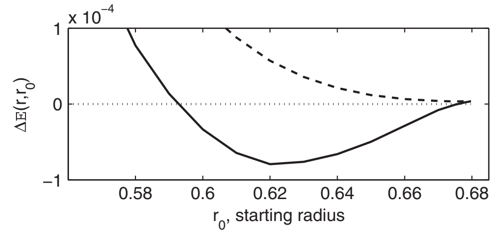

FIG. 5. Relative energy $\Delta\mathcal{E}$ evaluated from Eq. (6) for three equilibrium solutions $F'_\perp = 0$ of Eq. (4) in the region $0.58 < r_0 < 0.68$. The dotted line is the unperturbed energy, the dashed line is the unstable displaced equilibrium energy $[\Delta\mathcal{E}(r_{\mathrm{crit}}, r_0)]$, and the solid line is the displaced stable equilibrium energy $[\Delta\mathcal{E}(r_{\mathrm{sat}}, r_0)]$. The stable displaced equilibrium is the lowest energy state for $0.593 < r_0 < 0.679$.

We take an initial equilibrium with no linearly unstable field lines with $\alpha_0 = 0.28$, $s_0 = 0.05$, $s_1 = 0.3$, $r_a = 0.7$, $r_s = 0.72$, and $\epsilon_p = 0.1$. As r_0 is increased the equilibrium traces out the dash-dotted line in Fig. 3 in the direction indicated by the arrows. Clearly no surfaces (field lines) are linearly unstable and all infinitesimal perturbations decay. Nonetheless finite perturbations can grow. For example, in Fig. 4 we show the drag evolution $[r = r(\theta, r_0, t)$ using Eq. (4)] of the field line $r_0 = 0.61$ with two finite initial displacements. The larger initial displacement evolves to a finite displaced stable equilibrium. The smaller initial displacement decays to the linearly stable unperturbed state $r = r_0$ (Fig. 4). There are three equilibrium states of this field line that can be found by solving the equation $F'_\perp = 0$ [see Eq. (4)] by a simple shooting method. These are the linearly stable unperturbed state $r = r_0$ with relative energy $\Delta\mathcal{E} = 0$; an unstable equilibrium state $r = r_{\mathrm{crit}}(\theta, r_0)$ between the two initial conditions shown at $t = 0$ in

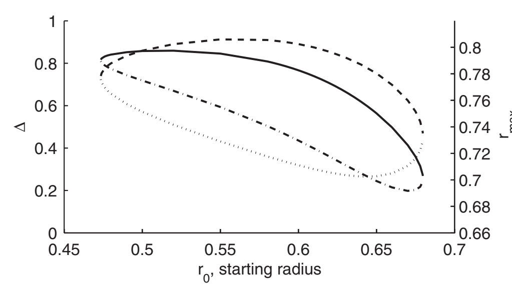

FIG. 6. A measure of the ballooning displacement $\Delta = [\beta_\alpha(r_0) - \beta_\alpha(r_{\max})]/(2\epsilon_p\alpha_0)$ for the two perturbed equilibrium states (left-hand axis). Field lines in the displaced lower energy equilibrium can cross a substantial fraction of the pressure profile (solid line)—for example, the $r_0 = 0.61$ field line balloons across about 73% of the pressure profile. The unstable equilibrium is shown by the dash-dotted line. The $r_{\max}$ for the saturated field lines is shown as the dashed line (right-hand axis) and the $r_{\max}$ for the unstable equilibria is shown as the dotted line. Note that for $0.56 < r_0 < 0.68$ the field lines "overtake," i.e., $r_{\max}(r_0^1) > r_{\max}(r_0^2)$ if $r_0^1 < r_0^2$.

Fig. 4 with $\Delta\mathcal{E} = 1.09 \times 10^{-4}$; and the stable equilibrium state $r = r_{\mathrm{sat}}(\theta, r_0)$ that is the final state of the larger perturbation with $\Delta\mathcal{E} = -0.8 \times 10^{-4}$. Clearly the unperturbed state is metastable since a finite perturbation triggers evolution to a lower energy state.

Not all the field lines have lower energy equilibrium states. We have examined the $F'_{\perp} = 0$ solutions for $0.4 < r_0 < 0.8$. For $0.474 < r_0 < 0.680$ there are three equilibrium solutions but outside this region the only equilibrium solution is the unperturbed state. All displaced solutions are even in θ and have their maximum displacement at $\theta = 0$, which we denote r_{max}. In Fig. 5 we plot $\Delta\mathcal{E}$ for $0.58 < r_0 < 0.68$ and in Fig. 6 we plot both $\Delta = [\beta_\alpha(r_0) - \beta_\alpha(r_{\mathrm{max}})]/(2\epsilon_p \alpha_0)$ (solid and dash-dotted lines, left-hand axis) and r_{max} (dashed and dotted lines, right-hand axis). Δ measures the fraction of pressure profile crossed by the ballooning flux tube. Clearly for $0.593 < r_0 < 0.678$ the lowest energy state is a displaced state (the solid black line in Fig. 5)—these states can be reached by giving the field line a perturbation with more than the energy of the unstable positive energy equilibrium state (the dashed line in Fig. 5).

We varied α_0 for this case; for $\alpha_0 \leq 0.269$ there are no energetically favorable saturated states, and for $\alpha_0 \geq 0.306$ some field lines are linearly unstable. It is not, however, the linearly unstable field lines that produce the saturated field lines with the largest displacement. These are metastable field lines with $r_0 \approx 0.6$. For a linearly unstable field line there are two lower energy saturated states, one displaced outwards and one inwards.

Discussion.—In this Letter we have formulated a nonlinear theory of ballooning modes as the eruption of elliptical flux tubes. The force in the direction of motion of the flux tube is given by combining pressure balance across the elliptical tube [Eq. (2)] with a generalized Archimedes principle [Eq. (3)]. We illustrate our theory with the drag evolution of flux tubes in a large aspect ratio circular flux surface equilibrium with an internal transport barrier—a nonlinear s-α model [10]. This model reveals remarkable physics. Even below the linear stability threshold there can be lower energy saturated flux tubes with finite displacement—we have found such states; see Fig. 5.

The flux tubes have been modeled with a perfectly conducting plasma. This is a reasonable assumption since the eruption is likely to take place on a fast time scale. Once the flux tubes have reached their saturated states then other, slower time scale processes become important. For example, resistive field line reconnection is likely to occur at large θ as it does in resistive ballooning modes [14]. There is also likely to be cross field transport of heat from the tube to the surrounding plasma around r_{max} given the large gradient of temperature. This would effectively connect the high pressure region to the low pressure region via a conduit ("hosepipe") along the flux tube—perhaps causing rapid loss of confinement locally. The balance of the dissipative processes determines the longer time scale evolution of the flux tube and ultimately how it disconnects from, or returns to, its original location.

ELMs are a possible application of the ideas in this Letter. However, we leave this topic to a future publication. We instead note that the explosive eruption of ballooning modes has been observed in TFTR shots with internal transport barriers [15]. A slowly evolving $n = 1$ kink mode arises first and then a toroidally localized ballooning mode (with $n \sim 10$–20) appears. These ballooning modes eventually disrupt the plasma—a hard limit. The tubes could be destabilized from a metastable state at the tip of the kink mode by finite noise or by passing through linear marginal stability. We have demonstrated with the model above that flux tubes can erupt into finitely displaced states effectively connecting plasma inside the transport barrier to outside the barrier. We speculate that the ballooning mode provides a hard limit when and only when there are finitely displaced lower energy saturated states. However, there is, clearly much to fathom before we can claim to fully understand the hard and soft limits of ballooning modes.

This work has received funding from the European Union's Horizon 2020 research and innovation program, Grant No. 633053, and from the RCUK Energy Programme (Grant No. EP/I501045). The views and opinions expressed herein do not necessarily reflect those of the European Commission. H. R. W. acknowledges the Royal Society's Wolfson Merit Award scheme.

† Christopher.ham@ukaea.uk
‡ Also at Department of Physics, Imperial College, Prince Consort Road, London SW7 2BZ, United Kingdom.

[1] T. C. Hender *et al.*, Nucl. Fusion **47**, S128 (2007).
[2] J. W. Connor, R. J. Hastie, and J. B. Taylor, Proc. R. Soc. A **365**, 1 (1979).
[3] J. W. Connor, J. B. Taylor, and M. Turner, Nucl. Fusion **24**, 642 (1984).
[4] H. R. Wilson, S. C. Cowley, A. Kirk, and P. B. Snyder, Plasma Phys. Controlled Fusion **48**, A71 (2006).
[5] P. B. Snyder, R. J. Groebner, J. W. Hughes, T. H. Osborne, M. Beurskens, A. W. Leonard, H. R. Wilson, and X. Q. Xu, Nucl. Fusion **51**, 103016 (2011).
[6] A. Kirk, B. Koch, R. Scannell, H. R. Wilson, G. Counsell, J. Dowling, A. Herrmann, R. Martin, and M. Walsh, Phys. Rev. Lett. **96**, 185001 (2006).
[7] S. C. Cowley and M. Artun, Phys. Rep. **283**, 185 (1997).
[8] H. R. Wilson and S. C. Cowley, Phys. Rev. Lett. **92**, 175006-1 (2004).
[9] S. C. Cowley, B. Cowley, S. A. Henneberg, and H. R. Wilson, Proc. R. Soc. A **471**, 20140913 (2015).
[10] J. W. Connor, R. J. Hastie, and J. B. Taylor, Phys. Rev. Lett. **40**, 396 (1978).
[11] J. W. Connor, S. C. Cowley, R. J. Hastie, T. C. Hender, A. Hood, and T. J. Martin, Phys. Fluids **31**, 577 (1988).
[12] J. M. Greene, J. L. Johnson, and K. E. Weimer, Phys. Fluids **14**, 671 (1971).

[13] S. C. Cowley, B. Cowley, S. A. Henneberg, and H. R. Wilson, Proc. R. Soc. A **471**, 20140913 (2015) (see Appendix B in arXiv:1411.7797).
[14] H. R. Struass, Phys. Fluids **24**, 2004 (1981).
[15] E. D. Fredrickson, K. M. McGuire, Z. Y. Chang, A. Janos, J. Manickam, G. Taylor, S. Mirnov, I. Semenov, D. Kislov, and D. Martynov, Phys. Plasmas **3**, 2620 (1996).